Inorganic Chemistry

Article

pubs.acs.org/IC

Comparative DNA Binding Abilities and Phosphatase-Like Activities of Mono-, Di-, and Trinuclear Ni(II) Complexes: The Influence of Ligand Denticity, Metal−Metal Distance, and Coordinating Solvent/Anion on Kinetics Studies

Vimal K. Bhardwaj*[,†] and Ajnesh Singh[‡]

[†]Department of Chemistry, Indian Institute of Technology Ropar, Rupnagar, Punjab 140001, India

[‡]Department of Applied Science and Humanities, Jawaharlal Nehru Government Engineering College, Sundernagar, Mandi, Himachal Pradesh 175010, India

Supporting Information

ABSTRACT: Six novel Ni(II) complexes, namely, $[Ni_2(HL^1)(OAc)_2]$ (**1**), $[Ni_3L^1{}_2]\cdot H_2O\cdot 2CH_3CN$ (**2**), $[Ni_2(L^2)(L^3)(CH_3CN)]$ (**3**), $[Ni_2(L^2)_2(H_2O)_2]$ (**4**), $[Ni_2(L^2)_2(DMF)_2]_2\cdot 2H_2O$ (**5**), and $[Ni(HL^2)_2]\cdot H_2O$ (**6**), were synthesized by reacting nitrophenol-based tripodal (H_3L^1) and dipodal (H_2L^2) Schiff base ligands with Ni(II) metal salts at ambient conditions. All the complexes were fully characterized with different spectroscopic techniques such as elemental analyses, IR, UV−vis spectroscopy, and electrospray ionization mass spectrometry. The solid-state structures of **2**, **3**, **5**, and **6** were determined using single-crystal X-ray crystallography. The compounds **1**, **3**, **4**, and **5** are dinuclear complexes where the two Ni(II) centers have octahedral geometry with bridging phenoxo groups. Compound **2** is a trinuclear complex with two different types of Ni(II) centers. In compound **3** one of the Ni(II) centers has a coordinated acetonitrile molecule, whereas in compound **4**, a water molecule has occupied one coordination site of each Ni(II) center. In complex **5**, the coordinated water of complex **4** was displaced by the dimethylformamide (DMF) during its crystallization. Complex **6** is mononuclear with two amine−bis(phenolate) ligands in scissorlike fashion around the Ni(II) metal center. The single crystals of **1** and **4** could not be obtained; however, from the spectroscopic data and physicochemical properties (electronic and redox properties) it was assumed that the structures of these complexes are quite similar to other analogues. DNA binding abilities and phosphatase-like activities of all characterized complexes were also investigated. The ligand denticity, coordinated anions/solvents (such as acetate, acetonitrile, water, and DMF), and cooperative action of two metal centers play a significant role in the phosphate ester bond cleavage of 2-hydroxypropyl-*p*-nitropenylphosphate by transesterification mechanism. Complex **3** exhibits highest activity among complexes **1**−**6** with 3.86×10^5 times greater rate enhancement than uncatalyzed reaction.

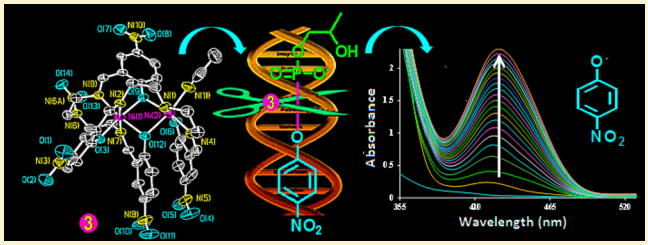

INTRODUCTION

Transition metal complexes of Schiff bases are of immense interest in homogeneous and heterogeneous catalysis.[1] They are known to catalyze oxygenation, hydrolysis, transesterification, and decomposition reactions.[2] Among these, the catalytic cleavage of phosphate esters either by hydrolysis or transesterification process has received considerable attention as an important biochemical process.[3] Phosphate esters are negatively charged species and show good resistance toward cleavage under neutral conditions. This special feature appears in the backbones of DNA and RNA. The hydrolytic enzymes such as polymerases, recombinases, and topoisomerases have two or three transition metal ions placed close to each other in their active sites.[4] These metal ions act as Lewis acid sites and facilitate catalysis by the cooperative action of two metal ions.[5] With the aim to mimic extraordinary catalytic activities of these enzymes, many binuclear model systems have been studied.[6] Model studies using phenoxo-bridged dinuclear metal complexes remain increasingly significant to recognize the importance of bimetallic centers.[7] We have already reported copper(II) acetate complexes of some Schiff bases and their reduced products and found them to have reasonable catecholase activity.[8] To continue our work on the bioinspired coordination chemistry of phenoxo-coordinated metal(II) complexes, we synthesized some new phenoxo-bridged complexes of Ni(II). The catalytic activity of these complexes toward phosphate ester bond cleavage was explored. The influence of ligand denticity and coordinated solvents or anions in the transesterification (catalytic bond cleavage) of organic phosphate ester was also investigated. Moreover, the binding of a metal complex to phosphate ester backbone, being a crucial step in transesterification, stimulated us to evaluate the DNA binding abilities of all the complexes before carrying out

Received: August 12, 2014
Published: September 16, 2014

   dx.doi.org/10.1021/ic501961d | *Inorg. Chem.* 2014, 53, 10731−10742

Scheme 1

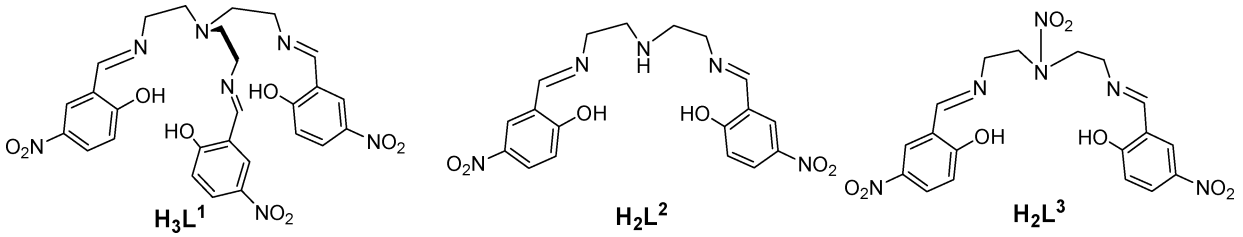

phosphate ester bond cleavage studies.[9] In the present work we are reporting six new complexes $[Ni_2(HL^1)(OAc)_2]$ (**1**), $[Ni_3L^1_2]\cdot H_2O\cdot 2CH_3CN$ (**2**), $[Ni_2(L^2)(L^3)(CH_3CN)]$ (**3**), $[Ni_2(L^2)_2(H_2O)_2]$ (**4**), $[Ni_2(L^2)_2(DMF)_2]_2\cdot 2H_2O$ (**5**), and $[Ni(HL^2)_2]\cdot H_2O$ (**6**) (DMF = dimethylformamide) from nitrophenol-based tripodal and dipodal Schiff base ligands. Although some similar complexes of **1** and **6** are known with Ni(II), none of them has ever been used for hydrolytic/transesterification cleavage studies.[10] The choice of nitrophenol-based ligand is based on the consideration that easy deprotonation of nitrophenol in comparison to phenol (due to lower pK_a value of nitrophenol, i.e., 7.2 as compared to 10.0 in case of phenol) will favor the complex formation. As expected, all the complexes were synthesized without the addition of any base. However, in case of phenolic ligands the complexation methods involve the use of some bases for deprotonation followed by metal complexation.[10,11] Further decrease in the number of coordination sites from tripodal ligand H_3L^1 to dipodal ligand H_2L^2 (Scheme 1) can favor the solvent or anion binding (such as water, acetonitrile, DMF, acetate, etc.) to complete the coordination sites of Ni(II) center. The crystal structure of complex **2**, **3**, and **5** has supported this anticipation. In contrast to our prediction we also isolated the complex **1** of tripodal ligand with bidentate-coordinated acetate ion. In spite of our sincere efforts we were unable to grow the crystals of this complex and assumed that the structure of complex **1** should resemble that of an already reported analogous complex. This argument was further confirmed by similarity in physiochemical properties (cf. electronic and redox properties) of complex **1** and those reported by Kennedy et al.[10] In case of complex **4** we were unable to grow the crystal in water again but succeeded in crystallizing the same compound in DMF as complex **5**, where coordinated water of complex **4** was displaced by DMF. We also isolated and characterized a mononuclear complex **6** to compare its activity with above-mentioned tri- and dinuclear complexes (**2**−**5**). Single crystals of **6** were also obtained; however, they could not provide publishable X-ray diffraction data. The proposed coordination environment of all the complexes is also supported with cyclic voltammetry. Therefore, these complexes are ideal candidates to study the influence of ligand denticity and exogenous coordinating ligands on DNA binding abilities and catalytic cleavage of phosphate esters. The relative DNA binding ability and catalytic activity of these complexes with appropriate mechanisms are finally reported.

EXPERIMENTAL SECTION

Materials and Measurements. All solvents were dried by standard methods. Unless otherwise specified, chemicals were purchased from commercial suppliers and used without further purification. calf thymus (CT)-DNA, ethidium bromide (EB), and biological buffers 2-[4-(2-hydroxyethyl)piperazin-1-yl] ethanesulfonic acid (HEPES), 4-(2-hydroxyethyl)-1-piperazinepropanesulfonic acid (EPPS), tetra-*n*-butyl ammonium perchlorate (TBAP), 2-(cyclohexylamino) ethanesulfonic acid (CHES), etc., were purchased from Aldrich. 2-hydroxypropyl-p-nitropenylphosphate (HPNP) was prepared by literature method.[12]

The elemental analyses were performed on Perkin−Elmer 2400 CHN analyzer. The ^{1}H and ^{13}C NMR spectra of the ligands were performed in $CDCl_3$ and deuterated dimethyl sulfoxide (DMSO-d_6) with tetramethylsilane (TMS) as an internal reference, on a JNM-ECS400 (JEOL) instrument operating at 400 MHz for ^{1}H NMR and 100 MHz for ^{13}C NMR. The chemical shifts are reported as δ values (ppm) relative to TMS. The IR spectra were recorded on a Bruker Tensor 27 spectrometer for the compounds in the solid state as KBr discs or as neat samples. The absorption spectra were recorded on a Specord 250 Plus Analytikjena and Agilent UV−vis spectrophotometer. The fluorescence measurements were performed on a PerkinElmer L55 Fluorescence spectrophotometer using quartz cells of 1 cm path length. The slit width for the excitation and emission was set at 10 nm, and scan speed was maintained at 100 scans per sec throughout the experiments. Electrospray mass spectra (ESI) were recorded on ES-MS Q-TOF mass spectrometer.

Syntheses of Ligands. Ligand (H_3L^1) and (H_2L^2) were prepared from tris(2-aminoethyl) amine and diethylenetriamine with a slight modification in the reported methods (Scheme 1).[13,14]

Ligand H_3L^1. Tris(2-aminoethyl) amine (146 mg, 1.0 mmol) was stirred with 2-hydroxy-5-nitrobenzlaldehyde (534.4 mg, 3.2 mmol) in the presence of traces of zinc perchlorate in methanol. Color of the solution changed immediately to yellow, and the precipitates separated out in quantitative yield. These precipitates were filtered, washed with methanol, and dried. Yield = 90.2%. mp = 197 °C. ^{1}H NMR (400 MHz, DMSO-d_6, ppm): δ 2.81 (m, 6H, $-CH_2$), 3.73 (m, 6H, $-CH_2$), 6.45 (d, 3H, Ar), 7.83 (d, 3H, Ar), 8.09 (s, 3H, Ar), 8.54 (s, 3H, −N═CH).^{13}C NMR (100 MHz, DMSO-d_6, ppm) δ: 50.0, 50.2, 113.3, 122.5, 128.8, 132.5, 167.3, 177.5. Anal. Calcd (%) for $C_{27}H_{27}N_7O_9$: C, 54.64; H, 4.59; N, 16.52. Found: C, 54.58; H, 5.51; N, 16.61. Selected IR (KBr, cm^{-1}) 3272 (w), 1655 (s), 1610 (s), 1548(s). ESI-MS (m/z): 594.2 [(M + 1)$^+$].

Ligand H_2L^2. The ligand H_2L^2 was prepared in a similar manner as H_3L^1, by stirring diethylenetriamine (103 mg, 1.0 mmol) with 2-hydroxy-5-nitrobenzlaldehyde (367.4 mg, 2.2 mmol) in the presence of traces of zinc perchlorate in methanol. Similarly, the color of the solution changed immediately to yellow, and precipitates separated out in quantitative yield. These precipitates were filtered, washed with methanol, and dried. Yield = 92.0%. mp = 182−186 °C. ^{1}H NMR (400 MHz, DMSO-d_6, ppm): δ 2.88 (t, 4H, $-CH_2$), 3.63 (t, 4H, $-CH_2$), 6.51 (d, 2H, Ar), 7.96 (d, 2H, Ar), 8.32 (s, 2H, Ar), 8.33 (s, 2H, −N═CH). ^{13}C NMR (100 MHz, $CDCl_3$, ppm): δ 48.3, 50.7, 114.4, 122.4, 128.8, 132.0, 133.6, 177.3. Anal. Calcd (%) for $C_{18}H_{19}N_5O_6$: C, 53.86; H, 4.77; N, 17.45. Found: C, 53.78; H, 4.71; N, 17.51. Selected IR (KBr, cm^{-1}) 3250 (w), 1699 (s), 1632 (s), 1542 (s). ESI-MS (m/z): 402.1 [(M + 1)$^+$].

Syntheses of Complexes. *$[Ni_2(HL^1)(OAc)_2]$ (**1**).* To a warm solution of H_3L^1 (593 mg, 1.0 mmol) in acetonitrile, an aqueous solution of $Ni(OAc)_2\cdot 4H_2O$ (498 mg, 2.0 mmol) was added. The reaction mixture was stirred at 70 °C for 2 h. Light brown precipitates were obtained, which were filtered and washed with acetonitrile. Yield: 52%. Anal. Calcd (%) for $C_{31}H_{31}N_7Ni_2O_{13}$: C, 45.02; H, 3.78; N, 11.86. Found: C, 44.97; H, 3.48; N, 11.39. Selected IR (KBr, cm^{-1}): 3480 (w) ν_{O-H}, 3002 (m) $\nu_{aromatic\ C-H}$, 2981(w) $\nu_{aliphatic\ C-H}$, 1633 (s) $\nu_{C=N}$, 1558 $\nu_{asym\ OCO}$, 1511 $\nu_{sym\ ONO}$, 1471 $\nu_{sym\ OCO}$, 1310 $\nu_{asym\ ONO}$,

dx.doi.org/10.1021/ic501961d | Inorg. Chem. 2014, 53, 10731−10742

Table 1. Crystal Data and Refinement Parameters of $[Ni_3L^1_2]\cdot H_2O\cdot 2CH_3CN$ (2), $[Ni_2(L^2)(L^3)(CH_3CN)]$ (3), and $[Ni_2(L^2)_2(DMF)_2]\cdot 2H_2O$ (5)

compound	2	3	5
empirical formula	$C_{58}H_{56}N_{16}O_{19}Ni_3$	$C_{38}H_{36}N_{12}O_{14}Ni_2$	$C_{42}H_{52}N_{12}O_{16}Ni_2$
M_w	1457.32	1002.21	1098.36
temperature [K]	293(2)	293(2)	293(2)
crystal system	triclinic	triclinic	monoclinic
space group	$P\bar{1}$	$P\bar{1}$	$P21/n$
a/ [Å]	11.8152(5)	10.2820(5)	9.4243(6)
b/ [Å]	12.1657(5)	11.0297(6)	14.7104(9)
c/[Å]	12.5479(5)	19.1468(10)	18.6857(13)
α/ [deg]	84.983(2)	99.617(2)	90.00
β/[deg]	62.572(2)	101.878(3)	98.867(2)
γ/ [deg]	72.841(2)	98.525(3)	90.00
V [Å^3]	1527.14(11)	2057.16(18)	2559.5(3)
Z	1	2	2
D_c [Mg m^{-3}]	1.585	1.616	1.425
μ/[mm^{-1}]	1.005	1.000	0.813
reflections collected	51282	44082	106740
data/restraints/parameters	6003/0/440	8014/0/597	5039/0/327
unique reflections, [R_{int}]	6003 [0.1207]	8014 [0.1690]	5039 [0.1014]
GOF = S_{all}	0.960	0.935	1.016
final R indices			
R_1, wR_2 [$I > 2\sigma I$]	0.0460, 0.0916	0.0782, 0.1527	0.0400, 0.1025
R_1, wR_2 (all data)	0.0926, 0.1023	0.2017, 0.1807	0.0701, 0.1178
$\Delta\rho$max/$\Delta\rho$min [Å^3]	0.405/−0.375	0.922/−0.388	0.753/−0.529

1270 δ_{C-H} 1126 ν_{C-N}. ESI-MS (m/z): 650.2 $[Ni(HL^1)+1]^+$. Electronic spectrum [λ_{max}, nm (ε, M^{-1} cm^{-1})]: (in DMF) 356 (11 900), 629 (br) (83), 991 (33).

$[Ni_3L^1_2]\cdot H_2O\cdot 2CH_3CN$ (2). A solution of $Ni(NO_3)_2\cdot 6H_2O$ (580 mg, 2.0 mmol) and $\mathbf{H_3L^1}$ (593 mg, 1.0 mmol) in acetonitrile was refluxed for 3 h to obtain a clear solution. After the completion of reaction, the solution was filtered to remove any solid particles. Subsequent slow evaporation of the acetonitrile solution at room temperature resulted in the formation of brown crystals, which were filtered and washed with methanol. Single crystals thus obtained were found to be suitable for X-ray structural studies. Yield: 54%. Anal. Calcd (%) for $C_{58}H_{56}N_{16}Ni_3O_{19}$: C, 47.80; H, 3.87; N, 15.38. Found: C, 47.87; H, 3.82; N, 15.42. Selected IR (KBr, cm^{-1}): 3485 (m) ν_{O-H}, 3024 $\nu_{aromatic\ C-H}$, 2861 $\nu_{aliphatic\ C-H}$, 1628 (s) $\nu_{C=N}$, 1582 $\nu_{sym\ ONO}$, 1308 $\nu_{asym\ ONO}$, 1290 δ_{C-H}, 1188 ν_{C-N}. ESI-MS (m/z): 706.2 $[Ni_2(L^1)]^+$. Electronic spectrum [λ_{max}, nm (ε, M^{-1} cm^{-1})]: (in DMF) 319 (15 300), 680 (70), 981(44).

$[Ni_2(L^2)(L^3)(CH_3CN)]$ (3). H_2L^2 (401 mg, 1.0 mmol) and $Ni(NO_3)_2\cdot 6H_2O$ (290 mg, 1.0 mmol) were added successively to acetonitrile. The resulting solution was refluxed for 2 h to obtain a clear solution. The suitable quality crystals were grown directly from the above solution by slow evaporation method and were then filtered and washed with methanol. Yield: 42%. Anal. Calcd (%) for $C_{38}H_{36}N_{12}Ni_2O_{14}$: C, 45.54; H, 3.62; N, 16.77. Found: C, 45.60; H, 3.58; N, 16.73. Selected IR (KBr, cm^{-1}): 3010 (w) $\nu_{aromatic\ C-H}$, 2852 (m) $\nu_{aliphatic\ C-H}$, 2310 (w) δ_{-CN}, 2295 (s) ν_{-CN}, 1610 (s) $\nu_{C=N}$, 1502 $\nu_{sym\ ONO}$, 1321$\nu_{asym\ ONO}$, 1252 (s), 1180 (s) ν_{C-N}. ESI-MS (m/z): 503.2 $[Ni(L^3)+1]^+$. Electronic spectrum [λ_{max}, nm (ε, M^{-1} cm^{-1})]: (in DMF) 325 (12 600), 665 (68), 964 (35).

$[Ni_2(L^2)_2(H_2O)_2]$ (4). An aqueous solution of $Ni(Cl)_2\cdot 6H_2O$ (238 mg,1.0 mmol) was added to a solution of H_2L^2 (401 mg, 1.0 mmol) in acetonitrile. The reaction mixture was refluxed at 70 °C giving light brown precipitates after 1 h. The solution was filtered and dried to afford a brown powder. Yield: 56%. Anal. Calcd (%) for $C_{36}H_{38}N_{10}Ni_2O_{14}$: C, 45.41; H, 4.02; N, 14.71. Found: C, 45.37; H, 4.08; N, 14.79. Selected IR (KBr, cm^{-1}): 3390 (m) ν_{O-H}, 2792 (w) $\nu_{aromatic\ C-H}$, 1682 (s) $\nu_{C=N}$, 1558 $\nu_{sym\ ONO}$, 1352 $\nu_{asym\ ONO}$, 1224 (s) δ_{C-H}, 1112 (s) ν_{C-N}. ESI-MS (m/z): 458.1 $[Ni(L^2)+1]^+$. Electronic spectrum [λ_{max}, nm (ε, M^{-1} cm^{-1})]: (in DMF) 327 (11 900), 646 (80), 1034 (27).

$[Ni_2(L^2)_2(DMF)_2]\cdot 2H_2O$ (5). The brown powder of complex **4** was dissolved in DMF, and suitable quality crystals were grown directly from the above solution by vapor diffusion with diethyl ether. Yield: 36%. Anal. Calcd (%) for $C_{42}H_{52}N_{12}O_{16}Ni_2$: C, 45.93; H, 4.77; N, 15.30. Found: C, 45.98; H, 4.79; N, 15.28. Selected IR (KBr, cm^{-1}): 3484(m) ν_{N-H}, 2978 (m) $\nu_{aromatic\ C-H}$, 2752 (w) $\nu_{aliphatic\ C-H}$, 1692, 1622 (s) ν_{C-O}, 1562 (s) $\nu_{C=N}$, 1510 $\nu_{sym\ ONO}$, 1312 $\nu_{asym\ ONO}$, 1245 δ_{C-H}, 1184 ν_{C-N}. ESI-MS (m/z): 663.2 $\{[Ni_2(L^2)(DMF)_2]^{2+}+1e\}$. Electronic spectrum [$\lambda_{max}$, nm ($\varepsilon$, M^{-1} cm^{-1})]: (in DMF) 342 (13 600), 690 (br) (42), 960 (29).

$[Ni(HL^2)_2]\cdot H_2O$ (6). To a solution of H_2L^2 (401 mg, 1.0 mmol) in acetonitrile (30 mL), an aqueous solution of $Ni(OAc)_2\cdot 4H_2O$ (249 mg, 1.0 mmol) was added. The solution was refluxed for 2 h. A brown colored solution was obtained, which was filtered and kept for slow evaporation to get crystalline material. Yield: 58%. Anal. Calcd (%) for $C_{36}H_{38}N_{10}NiO_{13}$: C, 49.28; H, 4.37; N, 15.96. Found: C, 49.32; H, 4.34; N, 15.98. Selected IR (KBr, cm^{-1}): 3498 (m) ν_{O-H}, 3125 (m) $\nu_{aromatic\ C-H}$, 2858 (w) $\nu_{aliphatic\ C-H}$, 1652 (s) $\nu_{C=N}$, 1590 $\nu_{sym\ ONO}$, 1388 $\nu_{asym\ ONO}$, 1254 (s) δ_{C-H}, 1116 (s) ν_{C-N}. ESI-MS (m/z): 859.7 $[Ni(HL^2)_2+1]^+$. Electronic spectrum [λ_{max}, nm (ε, M^{-1} cm^{-1})]: (in DMF) 364 (12 700), 728 (br) (79), 1016 (68).

X-ray Structure Determination. The X-ray diffraction data were collected on a Bruker X8 APEX II KAPPA CCD diffractometer at 100 K using graphite monochromatized Mo Kα radiation (λ = 0.710 73 Å). The crystals were positioned at 40 mm from the CCD, and the diffraction spots were measured using a counting time of 10 s. Data reduction and multiscan absorption were carried out using the APEX II program suite (Bruker, 2007). The structures were solved by direct methods with the SIR97 program[15] and refined using full-matrix least-squares with SHELXL-97.[16] Anisotropic thermal parameters were used for all non-H atoms. The hydrogen atoms of C−H groups were with isotropic parameters equivalent to 1.2 times those of the atom to which they were attached. All other calculations were performed using the programs WinGX[17] and PARST.[18] The molecular diagrams were drawn with DIAMOND and OLEX2.[19] Final R values together with selected refinement details are given in Table 1.

dx.doi.org/10.1021/ic501961d | Inorg. Chem. 2014, 53, 10731−10742

Cyclic Voltammetry. Electrochemical measurements were recorded on a BASI EPSILON. All studies were performed in a single compartment under nitrogen atmosphere at 100 mV s^{-1} scan rate (25 °C), with a Pt disk as the working electrode, Ag/AgCl as the reference electrode (3 M KCl), and Pt wire as the counter electrode. The working Pt electrode was polished with basic Al_2O_3–water slurry and was washed with ethanol. The solutions for analyses were prepared by dissolving 10 mg of each complex in 5 mL of 30% DMF solution along with tetrabutyl ammonium perchlorate (0.1 M) as the supporting electrolyte.

DNA Binding. The DNA binding abilities of all the complexes were examined by UV–vis and fluorescence spectroscopic studies in 50 mM Tris-HCl/NaCl buffered 10% DMF solution at 7.5 pH. The UV–vis titrations were performed with addition of increasing amount of CT-DNA (in Tris-HCl/NaCl buffer) to a fixed concentration of metal complex (100 μM). The concentration of CT-DNA was calculated from the extinction coefficient (ε = 6600 M^{-1} cm^{-1}) and absorbance intensity at 260 nm.[20] The decrease in the absorbance intensity with increased amount of DNA was plotted with nonlinear least-squares fitting analyses. The relative binding properties of complexes to CT-DNA were investigated with fluorescence spectroscopic methods using EB (1.25 μM) bound CT-DNA (25 μM) in 50 mM Tris-HCl/NaCl buffered 10% DMF solution at 7.5 pH. The decrease in the fluorescence intensity at ∼600 nm with an excitation wavelength of 525 nm was recorded with increasing amounts (0–30 μM) of different metal complexes.

Kinetics Measurements for Phosphate Ester Bond Cleavage. In all the kinetics studies for phosphate ester bond cleavage, 2-hydroxypropyl-*p*-nitropenylphosphate (HPNP) was used as substrate against all complexes. All the experiments were performed in spectroscopic grade 30% DMF solution (DMF–H_2O, v/v). Doubly distilled deionized water was used for the buffer preparation. A digital pH meter was used to measure the pH of different solutions. The 10 mL solution of each buffer salt (0.1 M) (HEPES, pH < 8.0; EPPS, 8.0 < pH < 8.9; CHES, 8.9 < pH < 11.0) was prepared and mixed with an equal volume of 0.2 M $NaNO_3$ solution (to maintain the ionic strength). These mixtures were titrated with NaOH (1 M) to get the desired pH. All the kinetics studies were performed on a UV–vis spectrophotometer fitted with a thermostated cuvette holder accessory, using the following conditions: The freshly prepared substrate solution (5.0 mM) was mixed with complex solution (0.1 mM) in an appropriate buffer. The rates of substrate transesterification in the presence of different complexes were measured by initial rate method at pH 8.5. The increase in absorption band (λ_{max} 400–410 nm) corresponding to the formation of *p*-nitrophenolate was recorded after every 3 min for 1 h. The effect of pH on catalytic activity was studied in the pH range of 7.0–10.0 using different buffer solutions. To determine the dependence of the rates on the substrate concentration and various kinetics parameters, 0.1 mM solutions of different metal complexes were treated with increasing substrate concentration (1.25–10 mM) in 30% DMF buffer solution at pH 8.5. The effect of acetate ion concentration on reaction rate was studied in the presence of 5 times of acetate ion relative to substrate concentration. In all the experiments UV spectra of solutions were recorded directly after 15 min equilibration time at 30 °C. All the measurements were recorded twice, and the average values were taken. The studies were corrected for spontaneous reaction by taking difference with and without metal complex. The mechanism of HPNP (2.5 mM) transesterification with complex **3** (0.1 mM) was studied by ^{31}P NMR spectroscopy in DMSO at pH 8.5, in the presence of 0.1 M CHES buffer. The formation of cyclic phosphodiester during transesterification reaction was confirmed by the appearance of a signal at 17.90 ppm.[21]

RESULTS AND DISCUSSION

Syntheses and Characterization. Phenol-based Schiff base ligands were synthesized with slight modification to reported methods[13,14] through the condensation reaction between tris(2-aminoethyl) amine/diethylenetriamine and 2-hydroxy-5-nitrobenzlaldehyde in methanol. The reactions of Schiff base ligands with different nickel salts afforded the separation of six complexes. All the complexes were fully characterized with different spectroscopic techniques such as elemental analyses, IR, UV–vis spectroscopy, and ESI mass spectrometry (Supporting Information, Figures S1–S12). The X-ray crystal structures of **2**, **3**, **5**, and **6** were also solved. IR spectra of all the complexes show −C═N stretching bands in the range of 1582–1652 cm^{-1}. Significant shifts in the ligand −C═N stretching band clearly shows its participation in coordination. In complex **1**, characteristic IR bands at 1558 and 1471 cm^{-1} were assigned to asymmetric and symmetric vibrations of coordinated acetate groups. The small separation $\Delta\nu$ between $\nu_{asym\ OCO}$ and $\nu_{sym\ OCO}$ (<200 cm^{-1}) suggests a bidentate chelating mode of coordinated acetate groups.[22] In complexes **3** and **4**, bands at 2295 and 3390 cm^{-1} show the presence of coordinated acetonitrile and water, respectively. Complex **5** shows a sharp band at 3484 cm^{-1} due to coordinated DMF.

The absorption spectra of complex **1** in DMF shows the characteristic features of an octahedral environment around two Ni(II) ions. The ground state ($^3A_{2g}$) of Ni(II) ion in an octahedral environment exhibits three spin-allowed transitions corresponding to $^3A_{2g} \rightarrow {}^3T_{1g}$ (F) (ν_1), $^3A_{2g} \rightarrow {}^3T_{2g}$ (F) (ν_2), and $^3A_{2g} \rightarrow {}^3T_{1g}$ (P) (ν_3) transitions.[23] Complexes **1**–**6** exhibit weak absorption bands in the range of 629–690 nm and 960–1034 nm in the visible region. The low intensity (ε = 27–83 M^{-1} cm^{-1}) and broadness of the absorption maxima are suggestive of the spin-forbidden transitions. The third high intensity band (ε = 11 800–15 300 M^{-1} cm^{-1}) at 319–364 nm, can be ascribed to the ligand-to-metal charge transfer transition. The high energy band corresponding to $^3A_{2g} \rightarrow {}^3T_{1g}$ (P) (ν_3) transition lies very close to the intense charge transfer band and has been overlapped. ESI-MS spectrum of nickel(II) complexes $[Ni_2(HL^1)(OAc)_2]$ (**1**), $[Ni_3L^1_2]\cdot H_2O\cdot 2CH_3CN$ (**2**), $[Ni_2(L^2)(L^3)(CH_3CN)]$(**3**), $[Ni_2(L^2)_2(H_2O)_2]$ (**4**), $[Ni_2(L^2)_2(DMF)_2]\cdot 2H_2O$ (**5**), and $[Ni(HL^2)_2]\cdot H_2O$ (**6**) showed a peak at m/z = 650.2 $[Ni(HL^1)+1]^+$, 706.2 $[Ni_2(L^1)]^+$, 503.2 $[Ni(L^3)+1]^+$, 458 $[Ni(L^2)+1]^+$, 663.2{$[Ni_2(L_2)(DMF)_2]^{2+}$+1e}, and 859.7 $[Ni(HL^2)_2+1]^+$, respectively. Moreover the proposed formulas of all the Ni(II) complexes are supported with elemental analyses and cyclic voltammetry.

Structure Description. *(a). $[Ni_3L^1_2]\cdot H_2O.2CH_3CN$ (2).* The compound **2** crystallizes in triclinic crystal system with $P\bar{1}$ space group. The asymmetric unit consists of one trinuclear Ni(II) complex $[Ni_3(C_{27}H_{24}N_7O_9)_2]$ and two acetonitrile, one water molecule as solvent of crystallization (Figure 1). There are two crystallographically different Ni(II) centers, namely, Ni(1) and Ni(2), of which Ni(2) is at the center of symmetry. The nickel atom has a slightly distorted octahedral coordination around Ni(1) center with three donor atoms (two phenolate oxygen atoms and one C═N nitrogen atom) from each tripodal ligand ($\mathbf{H_3L^1}$). The maximum deviation from the regular octahedral geometry is only in *cis*–N–Ni(1)–O (N2–Ni1–O4 = 94.64°) angles, while *trans*-N/O–Ni(1)–N/O angles are exactly 180°. In the second Ni(II) center, Ni(2) metal ion has distorted octahedral geometry (extent of distortion is more compared to Ni(1) center); the maximum deviation of *cis*-N/O–Ni–N/O angle is 15.54° from the ideal value of 90°. The corresponding deviation in the *trans*-N/O–Ni–N/O angle is as high as 14.34°. This distortion in octahedral geometry arises from two sterically hindered pods of tripodal ligand interacting with Ni(2) center leaving the third pod free to coordinate to Ni(1)

dx.doi.org/10.1021/ic501961d | *Inorg. Chem.* 2014, 53, 10731–10742

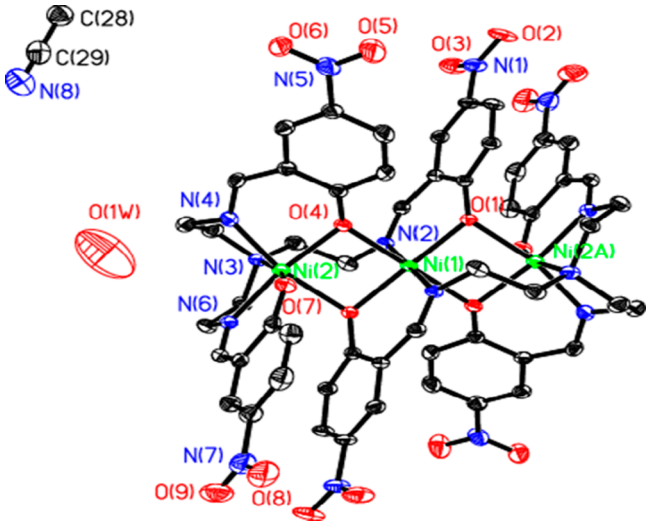

Figure 1. ORTEP diagram of $[Ni_3L^1_2]\cdot H_2O\cdot 2CH_3CN$ (**2**) with 40% probability thermal ellipsoids and the atom-numbering scheme (hydrogen atoms are removed for clarity).

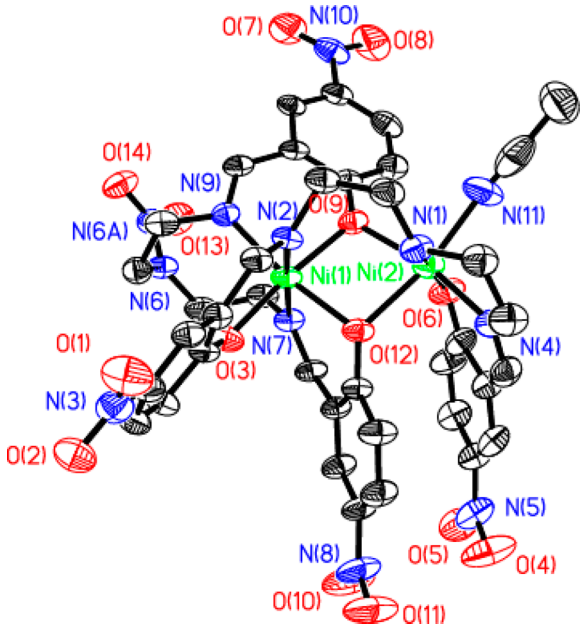

Figure 2. ORTEP diagram of $[Ni_2(L^2)(L^3)(CH_3CN)]$ (**3**). with 40% probability thermal ellipsoids and the atom-numbering scheme (hydrogen atoms are removed for clarity).

center. The average Ni−N, Ni−O distances around Ni(II) octahedrons are comparable to other similar reported Ni(II) complexes.[10] The selected bond lengths and bond angles are given in Table 2a. In the crystal lattice the different moieties are held together by weak C−H···O interactions, and all the oxygen atoms of the nitro groups are involved in hydrogen-bonding interactions with neighboring moieties (Supporting Information, Figure S13). The solvent molecules of crystallization are proving more robustness to the crystal structure by hydrogen-bonding interactions with metal complex moieties. The hydrogen-bonding interactions are shown in the Supporting Information, Table S1.

*(b). [$Ni_2(L^2)(L^3)(CH_3CN)$] (**3**).* Compound **3** crystallizes in triclinic crystal system with $P\bar{1}$ space group and consists of one dinuclear neutral Ni(II) complex, $[Ni_2(C_{18}H_{17}N_5O_6)(C_{18}H_{16}N_6O_8)CH_3CN]$. Interestingly, dipodal ligands coordinating to Ni(II) are different, in one dipodal ligand ($\mathbf{H_2L^2}$) the central nitrogen atom (N6) has undergone nitrosation reaction (ligand $\mathbf{H_2L^3}$, Scheme 1) during complexation in the presence of nitrate ion (counterion of Ni(II) salt), while central nitrogen atom (N1) of other dipodal ligand ($\mathbf{H_2L^2}$) is involved in coordination with Ni(II) metal center. The ORTEP diagram along with atom numbering scheme is shown in Figure 2. In compound **3**, both nickel atoms are hexacoordinated resulting in octahedral geometry around metal centers. In Ni(1), octahedral coordination is completed by three nitrogen and three phenolate oxygen atoms originating from two dipodal ligands. Around Ni(2) metal center the octahedral geometry is completed by two nitrogen, three oxygen donor atoms of two dipodal ligands, while the sixth position is satisfied by one acetonitrile ligand. The compound has nearly octahedral geometry around the metal centerrs, the maximum deviation of *cis*-N/O−Ni−N/O angle is 11.45° from the ideal value of 90°. The corresponding deviation in the *trans*-N/O−Ni−N/O angle is as low as 14.7°. The average Ni−N, Ni−O distances around Ni(II) octahedron are comparable to those of other related Ni(II) complexes and are given in Table 2b.

In the crystal lattice the Ni(II) moieties are interacting with each other through number of C−H···O hydrogen bonding. The resulting arrangement as shown in Supporting Information, Figure S14, propagates toward one direction with help of hydrogen-bonding interactions between two nitrophenolate units, which are almost perpendicular to two other nitrophenolate units of dipodal ligands. The arrangement is propagating toward other direction by C−H···O interactions

Table 2a. Selected Bond Lengths (Å) and Angles (deg) for $[Ni_3L^1_2]\cdot H_2O\cdot 2CH_3CN$ (2)

bond lengths (Å)					
Ni(1)−O(1)	2.026(2)	Ni(1)−N(2)	2.069(3)	Ni(1)−O(4)	2.165(2)
Ni(2)−N(4)	2.001(3)	Ni(2)−N(6)	2.036(3)	Ni(2)−O(7)	2.013(2)
Ni(2)−N(3)	2.249(3)	Ni(2)−O(4)	2.056(2)	N(1)−O(2)	1.230(4)
N(1)−O(3)	1.237(4)	N(5)−O(6)	1.231(4)	N(5)−O(5)	1.224(4)
N(7)−O(9)	1.225(4)	N(7)−O(8)	1.231(4)	Ni(1)···Ni(2)	3.214
bond angles (deg)					
O(1)−Ni(1)−N(2)	90.29(9)	O(1)−Ni(1)−O(4)	98.79(8)	N(2)−Ni(1)−O(4)	85.38(9)
N(4)−Ni(2)−N(3)	78.59(11)	O(4)−Ni(2)−N(3)	105.53(9)	O(7)−Ni(2)−O(4)	85.87(9)
O(5)−N(5)−O(6)	123.2(3)	O(7)−Ni(2)−N(6)	89.24(10)	N(6)−Ni(2)−O(4)	170.56(10)
N(4)−Ni(2)−O(7)	96.36(10)	O(7)−Ni(2)−N(3)	167.25(10)	N(6)−Ni(2)−N(3)	80.25(10)
N(4)−Ni(2)−O(4)	88.41(10)	N(4)−Ni(2)−N(6)	100.16(11)	O(1)−Ni(1)−O(4)#1	81.21(8)
O(2)−N(1)−O(3)	123.4(3)	O(5)−N(5)−O(6)	123.2(3)	O(9)−N(7)−O(8)	123.4(4)

dx.doi.org/10.1021/ic501961d | *Inorg. Chem.* 2014, 53, 10731−10742

Table 2b. Selected Bond Lengths (Å) and Angles (deg) for $[Ni_2(L^2)(L^3)(CH_3CN)]$ (3)

bond lengths (Å)					
Ni(1)−O(3)	1.995(4)	Ni(1)−N(2)	2.092(4)	Ni(2)−N(11)	2.043(6)
Ni(1)−N(9)	2.047(5)	Ni(1)−N(7)	2.101(4)	Ni(2)−O(9)	2.086(4)
Ni(1)−O(9)	2.052(4)	Ni(2)−O(6)	1.987(4)	Ni(2)−N(1)	2.109(5)
Ni(1)−O(12)	2.052(4)	Ni(2)−N(4)	2.016(5)	Ni(2)−O(12)	2.173(4)
bond angles (deg)					
O(3)−Ni(1)−N(9)	96.27(18)	O(3)−Ni(1)−N(7)	88.12(16)	N(11)−Ni(2)−O(9)	95.1(2)
O(3)−Ni(1)−O(9)	174.02(16)	N(9)−Ni(1)−N(7)	96.73(18)	O(6)−Ni(2)−N(1)	170.16(19)
N(9)−Ni(1)−O(9)	89.64(17)	O(9)−Ni(1)−N(7)	90.26(16)	N(4)−Ni(2)−N(1)	80.9(2)
O(3)−Ni(1)−O(12)	92.01(16)	O(12)−Ni(1)−N(7)	86.66(16)	N(11)−Ni(2)−N(1)	88.0(3)
N(9)−Ni(1)−O(12)	171.14(17)	N(2)−Ni(1)−N(7)	174.74(18)	O(9)−Ni(2)−N(1)	98.93(17)
O(9)−Ni(1)−O(12)	82.15(15)	O(6)−Ni(2)−N(4)	89.4(2)	O(6)−Ni(2)−O(12)	98.65(16)
O(3)−Ni(1)−N(2)	89.68(16)	O(6)−Ni(2)−N(11)	94.7(3)	N(4)−Ni(2)−O(12)	89.79(18)
N(9)−Ni(1)−N(2)	88.27(17)	N(4)−Ni(2)−N(11)	96.7(3)	N(11)−Ni(2)−O(12)	165.3(3)
O(9)−Ni(1)−N(2)	91.44(16)	O(6)−Ni(2)−O(9)	90.29(16)	O(9)−Ni(2)−O(12)	78.55(14)
O(12)−Ni(1)−N(2)	88.63(16)	N(4)−Ni(2)−O(9)	168.16(18)	N(1)−Ni(2)−O(12)	79.99(17)

between C/N−H and oxygen atoms of nitrophenolate moieties. Hydrogen-bonding parameters are reported in Supporting Information, Table S2. The C−H···π interactions were observed between centroid of nitrophenolate moiety and C−H of acetonitrile ligand (C−H···Cg = 2.901 Å, angle C−H···Cg = 118.19° where Cg is centroid of ring defined by C4−C9).

*(c). $[Ni_2(L^2)_2(DMF)_2]\cdot 2\ H_2O$ (**5**).* Compound **5** crystallizes in monoclinic crystal system with $P2_1/n$ space group and consists of one dinuclear neutral Ni(II) complex, $[Ni_2(C_{18}H_{17}N_5O_6)_2(DMF)_2]$ with two guest water molecules in the lattice. The ORTEP diagram along with atom numbering scheme is shown in Figure 3. In compound **5**, the nickel atom,

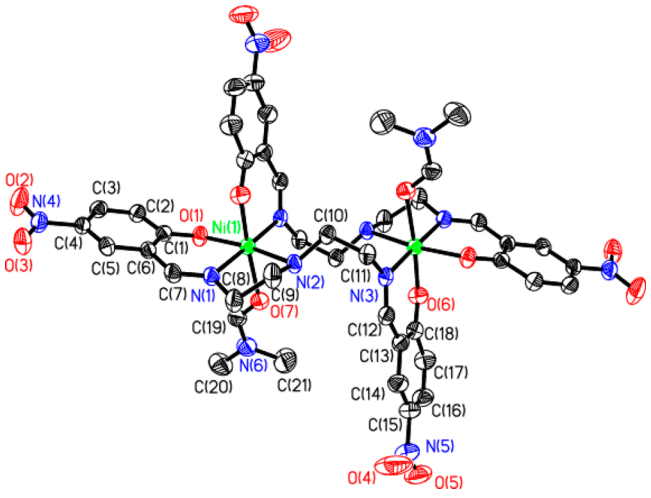

Figure 3. ORTEP diagram of $[Ni_2(L^2)_2(DMF)_2]\cdot 2H_2O$ (**5**) with 40% probability thermal ellipsoids and the atom-numbering scheme (hydrogen atom and water molecules are removed for clarity).

which lies on a symmetry center, is hexacoordinated to two dipodal ligands and one dimethylformamide molecule at the apexes of an elongated octahedron. Two nitrogen atoms and one oxygen atom are originated from one ligand, while one nitrogen atom and one oxygen atom are coordinating to the Ni(II) center from one pod of other ligand. The $[Ni_2(C_{18}H_{16}N_5O_6)_2(DMF)_2]$ complex has nearly octahedral geometry around the metal center, and the maximum deviation of the *cis*-N/O−Ni−N/O angle is 10.43° from the ideal value of 90°. The corresponding deviation in the *trans*-N/O−Ni−N/O angle is as low as 9.51°. The average Ni−N, Ni−O distances around Ni(II) octahedron are 2.034 (2), 2.054 (2)Å, respectively. The structural parameters of the complex **5** with those of other related Ni(II) complexes[11] showed a substantial agreement for bond lengths and angles as given in Table 2c.

In the crystal lattice the Ni(II) moieties are arranged in chains running along *b*-axis where subsequent Ni(II) moieties are interacting with each other through O−H···O and C−H···O hydrogen bonding (Supporting Information, Figure S15). The lattice water molecules are acting as linker between two Ni(II) moieties. The hydrogen bond acceptor groups (oxygen atoms) originating from nitro groups of the ligands are involved in O/C−H···O bonding to extend these chains in the three-dimensional lattice. Hydrogen-bonding parameters are reported in Table S3 in Supporting Information)

*(d). $[Ni(HL^2)_2]\cdot H_2O$ (**6**).* The structure of compound **6** could not be refined to an acceptable publishable level because of poor diffraction and solvent disorder. However, the connectivity of mononuclear complex can be clearly established from these data. An ORTEP representation and crystal data and refinement parameters of complex **6** is given in Supporting Information (Figure S16, Table S4). Compound **6** consists of one mononuclear neutral Ni(II) complex, $[Ni(C_{18}H_{18}N_5O_6)_2]$ with guest water molecule in the lattice. The Ni(II) ion of the complex is hexacoordinated with two amine−bis(phenolate) ligands in scissorlike fashion. The metal center is coordinated by the phenolate oxygen atoms (O1 and O4) and imine nitrogen atoms (N1 and N3) of two separate ligands. The fifth and sixth coordination site of Ni(II) is satisfied by two central amine nitrogen atoms (N4 and N6) of both the ligands. The bond angles around Ni(II) show a small deviation from the octahedral geometry around the metal ion; selected bond lengths and bond angles are given in Supporting Information, Table S5.

Electrochemical Properties. To study the redox properties of the central metal ions, electrochemical experiments were performed for complexes **1**−**6** in 30% DMF−H_2O solution. In the negative potential region the complexes **1**−**5** exhibit two quasireversible reduction waves at E^1_{pc} = −0.61 to −0.9 V and E^2_{pc} = −1.03 to −1.58 V corresponding to $Ni^{II}Ni^{II}$/ $Ni^{II}Ni^{I}$ and $Ni^{II}Ni^{I}$/ $Ni^{I}Ni^{I}$ redox process (Figure 4 and Supporting Information, Figure S17). Consequently these observations suggest a two-step redox process, which was suggested as follows.

dx.doi.org/10.1021/ic501961d | *Inorg. Chem.* 2014, 53, 10731−10742

Table 2c. Selected Bond Lengths (Å) and Angles (deg) for $[Ni_2(L^2)_2(DMF)_2]\cdot 2H_2O$ (5)

		bond lengths (Å)			
Ni(1)−N(1)	2.020(2)	Ni(1)−O(1)	2.039(2)	Ni(1)−O(7)	2.126(2)
Ni(1)−N(2)	2.153(2)	Ni(1)−O(6)#1	1.999(2)	Ni(1)−N(3)#1	2.069(2)
O(2)−N(4)	1.235(3)	O(3)−N(4)	1.223(3)	O(1)−C(1)	1.291(3)
Ni(1)···Ni(1)	5.722				
		bond angles (deg)			
O(6)#1−Ni(1)−N(1)	90.26(8)	O(6)#1−Ni(1)−O(1)	92.23(8)	N(1)−Ni(1)−O(1)	88.08(8)
N(1)−Ni(1)−N(3)#1	177.02(9)	O(1)−Ni(1)−N(3)#1	89.07(7)	O(6)#1−Ni(1)−O(7)	173.38(8)
O(1)−Ni(1)−O(7)	94.12(8)	N(3)#1−Ni(1)−O(7)	91.29(8)	O(6)#1−Ni(1)−N(2)	88.30(9)
N(1)−Ni(1)−N(2)	82.41(8)	O(1)−Ni(1)−N(2)	170.49(7)	N(3)#1−Ni(1)−N(2)	100.43(8)
O(7)−Ni(1)−N(2)	85.12(9)	O(4)−N(5)−O(5)	122.7(4)	O(4)−N(5)−C(15)	118.6(4)
O(5)−N(5)−C(15)	118.7(4)				

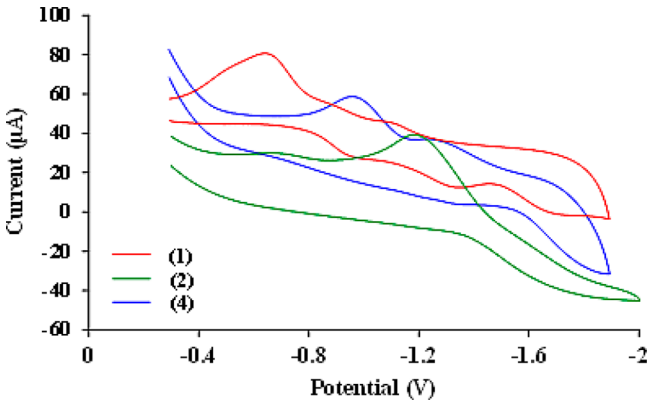

Figure 4. Cyclic voltammogram of complex **1**, **2**, and **4** (negative potential region) in 30% DMF−H_2O solution.

The redox behavior of mononuclear complex **6** showed one irreversible reduction wave at $E^1_{pc} = -0.65$ V, corresponding to Ni^{II}/Ni^{I} redox process. During the redox cycle there is decrease in the charge of the complex from +2 to +1, which may be assigned to the reduction of first Ni(II) ion. Conceptually the reduction of electron density on the central metal ions by coordinated moieties reduces the metal ion at less negative potential and vice versa.[24] Hence the Ni(II) ion in complex **1** reduces at relatively low negative potential ($E^1_{pc} = -0.62$ V) due to lesser electron density on the metal ion (due to coordinated acetate group) as compared to complex **2** ($E^1_{pc} = -0.66$ V) with three nitrophenolate coordination sites. Complex **4** reduces at highest negative potential ($E^1_{pc} = -1.09$ V) due to the presence of coordinated water molecule. As per literature reports[6h] the pK_a value of coordinated water is ∼7.78−8.78 in nickel complexes,; this accounts for the deprotonation of coordinated water to OH^- ion in complex **4**. The highest pK_a of OH^- ion (pK_a of $CH_3COO^- < NO_2C_6H_4O^- < OH^-$) leads to the reduction of complex **4** at highest negative potential ($E^1_{pc} = -1.09$ V). On the other hand in trinuclear complex **2** the reduction process is fast enough, leading to the appearance of two redox peaks at $E^1_{pc} = -0.66$ and $E^2_{pc} = -1.20$ V, instead of expected three peaks. A similar behavior is also observed in the complexes **3**, **5**, and **6**. The electrochemical data of all the complexes is summarized in Table 3. In the positive potential region all the complexes (**1**−**6**) exhibit reversible and quasireversible oxidative responses at $E^1_{pa} = +0.12$ to $+0.48$ V and $E^2_{pa} = +0.18$ to $+0.77$ V, respectively (Supporting Information, Figure S18). A slight anodic shift was observed in the oxidation waves with decrease in electron density around central metal ion. The observed redox process in this positive region can be assigned to the stepwise oxidation of Ni(II) ion.

DNA Binding Studies. The DNA binding aptitude of all the complexes (100 μM) was studied by performing absorbance (UV−vis) titrations with CT-DNA (0−50 μM) in Tris-HCl/NaCl buffered 10% DMF solution at 7.5 pH. UV−vis absorption titrations showed a gradual decrease in the absorbance intensity (charge transfer band) of all the complexes, with incremental addition of CT-DNA (Figure 5 and Supporting Information, Figure S19). The strength of binding is directly related to the extent of decrease in intensity; with more hypsochromism, stronger will be the binding. The intrinsic binding constants were also determined from the titration results with the following equation.

$$[DNA]/(\varepsilon_a - \varepsilon_f) = [DNA]/(\varepsilon_a - \varepsilon_f) + 1/K_b(\varepsilon_b - \varepsilon_f)$$

where ε_a is the extinction coefficient (charge transfer band) of Ni(II) complex for a particular DNA concentration, ε_f is the extinction coefficient of free complex, and ε_b is the extinction coefficient of Ni(II) complex in fully bound form. The binding constants (K_b) for all the complexes are given in Table 4. The low values of binding constants (∼10^4 M^{-1}) suggested the nonintercalative mode of DNA binding.[25] Hence the binding between complex and DNA is only through electrostatic

Table 3. Electrochemical Data of 1−6 Ni(II) Complexes

	reduction process						oxidation process				
	E^1_{pc} (V)	E^1_{pa} (V)	$E^1_{1/2}$ (V)	E^2_{pc} (V)	E^2_{pa} (V)	$E^2_{1/2}$ (V)	E^1_{pa} (V)	E^2_{pa} (V)	E^2_{pc} (V)	$E^1_{1/2}$ (V)	$E^2_{1/2}$ (V)
1	−0.62	−0.9	−0.41	−1.03	−1.30	−1.00	+0.48	+0.77	+0.24	+0.32	+0.72
2	−0.66		−0.58	−1.20	−1.18	−1.12	+0.32	+0.55	+0.22	+0.29	+0.50
3	−0.76	−6.2	−0.71	−1.58	−1.52	−1.55	+0.33	+0.57	+0.36	+0.23	+0.53
4	−0.90		−0.84	−1.24	−1.21	−1.10	+0.12	+0.66	+0.24	+0.07	+0.61
5	−0.82	−0.92	−0.80	−1.24		−1.21	+0.31	+0.57	+0.32	+0.22	+0.55
6	−0.65	−1.6	−0.53				+0.4	+0.18		+0.32	

dx.doi.org/10.1021/ic501961d | Inorg. Chem. 2014, 53, 10731−10742

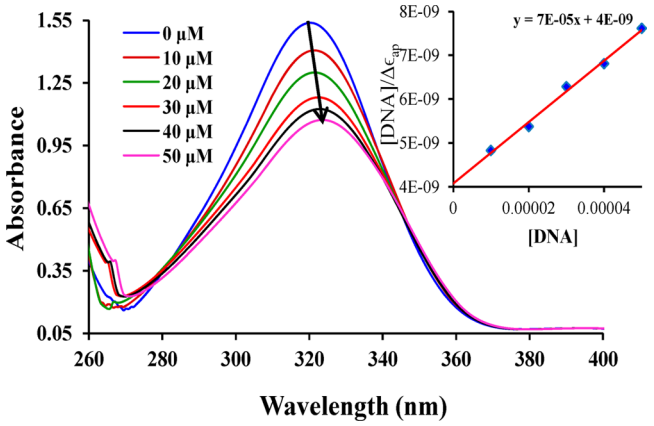

Figure 5. Absorption spectral changes at 319 nm (ε = 15 300 M^{-1} cm^{-1}) upon the incremental addition of CT-DNA (0−50 μM) to complex **2** (100 μM, 1.0 mL) in 50 mM Tris-HCl/NaCl buffered 10% DMF solution (7.5 pH) at room temperature. (inset) Plot of [DNA]/$\Delta\varepsilon$ versus [DNA] obtained by the absorption titration of CT-DNA with Ni(II) complex.

interactions in which the positive charge of metal ion assists the complex to interact with negatively charged phosphodiester backbone of DNA. The binding constants of all the complexes follow the order **2** > **1** > **3** > **5** > **4** > **6** (Supporting Information, Figure S20).

The trinuclear complex **2** showed highest value of K_b among all the complexes due to structurally more favorable binding. The presence of three metal centers provides enough rigidity to the complex that favors the stronger interaction between complex and DNA than other di- or mononuclear complexes.[26] Moreover the three metal centers in **2** have 6+ charge in comparison to 4+ or 2+ in other dinuclear and mononuclear complexes. Complex **1** also showed better binding than complexes **3**−**6** due to relatively rigid structure.[27] In complex **4**, two coordinated water molecules undergo depronation to OH^- ion, and the complex may have less positive charge than 4+, which results in the smaller value of DNA binding constant. Complex **6** has smallest value of binding constant due to its mononuclear structure and nonrigid nature. To confirm the electrostatic nature of DNA binding, the K_b values of complex **2** were compared in the absence and presence of 100 mM NaCl solution in 20 mM phosphate buffer at 7.5 pH. A significant decrease in the binding constant was observed from 1.75 × 10^4 to 7.5 × 10^3 upon NaCl addition (Supporting Information, Figure S21) due to decrease in the positive charge of the complex.

Similarly, fluorescence spectral titrations were also performed to study the binding affinity of tripodal complexes **1**−**3** for CT-DNA. As mentioned in Experimental Section, fluorescent emission of ethidium bromide (EB) is used as optical probe. The DNA binding affinity of metal complex was compared with EB-DNA complex. The emission intensity of EB increases when EB binds to DNA and decreases when EB releases DNA. The interaction of metal complex to DNA leads to non-availability of free DNA for EB; as a result, the fluorescence intensity of EB-DNA complex decreases. Therefore, the quenching of fluorescence intensity of EB-DNA system in the presence of metal complex can be used as tool for measuring the extent of DNA binding. In a typical experiment the solution of complex was added to EB-bound DNA. Complexes **1** and **2** showed the decrease in the emission intensity of EB-DNA system at 604 nm. The course of reaction with a solution of **2** is shown in Figure 6. On the basis of fluorescence curves, I_o/I

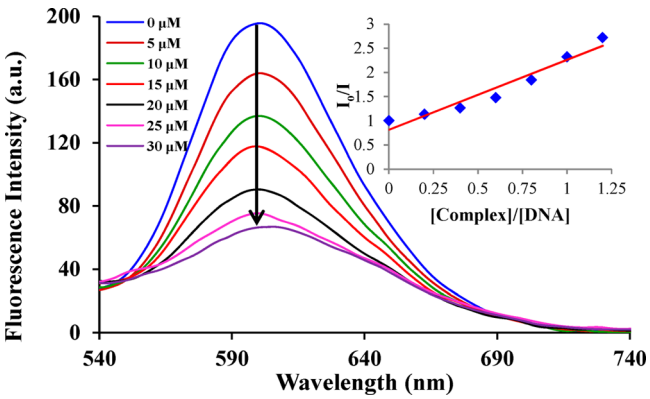

Figure 6. Fluorescence spectrum of EB (1.25 μM) bound to CT-DNA (25 μM) with increasing amounts of complex **2** (0−30 μM) at 604 nm (λ_{ex} = 525 nm) in 50 mM Tris-HCl/NaCl buffered 10% DMF solution (7.5 pH) at room temperature. (inset) Plot of emission intensity I_0/I vs [complex]/[DNA].

versus [complex]/[DNA] was plotted, where I_o is intensity of EB-bound DNA and I is the intensity of EB-bound DNA upon addition of complex (Supporting Information, Figure S22). The K_{app} values (apparent binding constant) were also calculated for complex **1** and **2** using literature method.[28]

$$K_{EB}[EB] = K_{app}[complex]$$

where [complex] corresponds to 50% reduction of emission intensity of EB-bound DNA, and K_{EB} = 1.0 × 10^7 M^{-1}, [EB] = 1.3 μM. The emission intensity of EB-bound DNA system was plotted against different concentration of metal complexes as in Supporting Information, Figure S23. The complex concentrations corresponding to 50% reduction of emission intensity were found and further used to calculate the K_{app} for each complex. The apparent DNA binding constants for **1** and **2** were found as 9.62 × 10^5 and 14.1 × 10^5 M^{-1}, respectively.

Phosphate Ester Cleavage Studies and Kinetics. There are a many reports in literature in which labile coordination site of dinuclear transition metal complex assist the hydrolysis/transesterification of phosphate esters.[6] The deprotonated metal-bound species such as OH^-/H_2O provides an appropriate nucleophile. The nucleophilic attack of metal-coordinated solvent and formation of cyclic transition state favor the intramolecular transesterification of HPNP to corresponding *p*-nitrophenolate product. The catalytic activity for the transesterification of DNA model substrate, that is, 2-hydroxypropyl-*p*-nitropenylphosphate (HPNP), were performed with all the complexes **1**−**6** (synthetic models). The catalytic efficiency of these complexes was determined using the method of pseudo-

Table 4. Binding Constants (K_b) of Complexes 1−6

complex	1	2	3	4	5	6
K_b (M^{-1})	1.0 × 10^4	1.75 × 10^4	8.5 × 10^3	2.0 × 10^3	4.2 × 10^3	5.0 × 10^2

dx.doi.org/10.1021/ic501961d | *Inorg. Chem.* 2014, 53, 10731−10742

first-order rate constants (k_{obs}) by monitoring the growth of *p*-nitrophenolate absorption band (425 nm, $\varepsilon = 1.65 \times 10^4$ M^{-1} cm^{-1}) as a function of time (in 30% DMF solution and pH 8.5 at 30 °C). All the complexes showed activity toward the transesterification of HPNP. After the addition of substrate to the solutions of the catalysts **1** to **6**, a new band corresponding to *p*-nitrophenolate appeared at 425 nm ($\varepsilon = 1.65 \times 10^4$ M^{-1} cm^{-1}). The course of a typical reaction with a solution of complex **3** is shown in Figure 7.

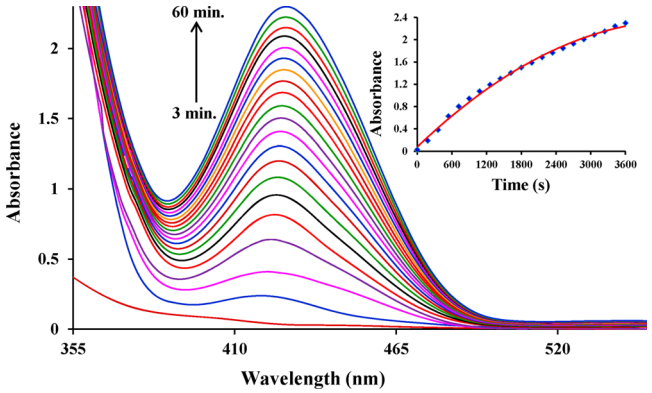

Figure 7. Absorption spectra for the transesterification of HPNP (5 mM) in the absence and presence of complex **3** (50 μM) (substrate/complex = 50:1) in 30% DMF recorded at an interval of 3 min at 30 °C. (inset) Absorption profile due to the formation of *p*-nitrophenolate (λ_{max} = 425 nm) on addition of HPNP to complex **3**.

The subsequent increase in absorbance of this band is linear for all the complexes. The initial first-order rate constants for catalytic phosphate ester cleavage were determined from the slope of a plot of $\log[A_\alpha/(A_\alpha - A_t)]$ versus time (Figure 8). It is

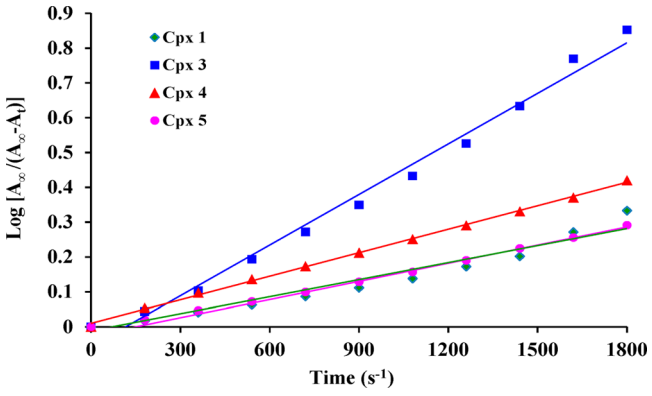

Figure 8. Plot of $\log[A_\infty/(A_\infty - A_t)]$ vs time to determine the first-order rate constants for HPNP transesterification reaction.

evident from Figure 8 that the complexes **1**, **3**, **4**, and **5** exhibit significant catalytic activity. The activity of all complexes differs considerably from each other, where complex **3** showed a maximum activity, and complexes **2** and **6** showed almost negligible activity.

To determine the dependence of the rates on the substrate concentration, all the complexes were treated with different concentrations of HPNP (1.25–10 mM). Initially a first-order dependence of the substrate concentration was observed. At higher concentrations, saturation kinetics was found, and first-order rate kinetics gradually deviated from unity for all the active compounds (Figure 9). The effect of concentration is more pronounced for **3** and **4** in contrast to other complexes

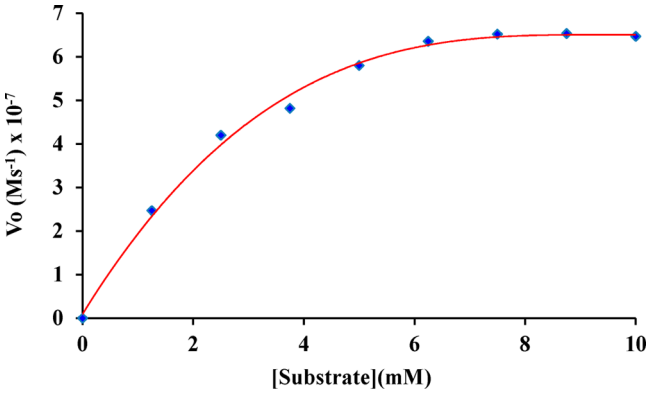

Figure 9. Dependence of rate of reaction on substrate concentration (0–10 mM) for complex **3** (50 μM) at 25 °C in 30% DMF (pH 8.5).

(Supporting Information, Figure S24). The dependence of rate on the substrate concentration suggests a catalyst–substrate binding to be an initial step in the catalytic mechanism.

The rates of reactions for various substrate concentrations were fitted to the Michaelis–Menten equation and linearized by means of Lineweaver–Burk plot (Figure 10) to calculate

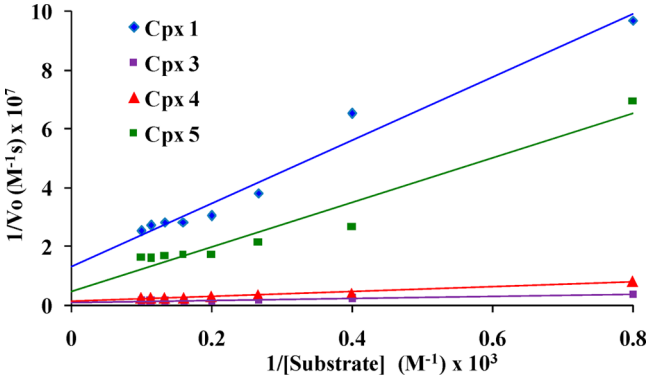

Figure 10. Lineweaver–Burk plot for the HPNP transesterification by complexes **1**, **3**, **4**, and **5**.

kinetics parameters (Table 5) for these complexes. To confirm the role of complexes in transesterification, the activities of all the complexes were compared with a blank solution (without Ni(II) complex). A very low spontaneous rate was observed in blank solution in the range of 10^{-8} s^{-1}.

The effect of pH on catalytic activity was also studied in the pH range of 7.0–10.0 for complexes **3** and **4.** The plot of rate versus pH (Figure 11 and Supporting Information, Figure S25) shows that the rate of transesterification significantly depends upon the pH of the solution. The reaction rate increases with increase in pH and finally gets saturated at higher pH 10. The complexes show a very low activity at pH 7, which slightly increases at pH 8 and becomes maximum at pH 9.5–10.0. The observed sigmoid-shaped rates versus pH curves are characteristic of an acid–base equilibrium-controlled kinetics process. This pH-dependent rate constant suggests that deprotonation of a metal-bound species favors the generation of catalytically active nucleophiles. In a typical ester cleavage process for any complex to act as an efficient catalyst, the incoming substrate first binds effectively to the catalyst. The substrate further

dx.doi.org/10.1021/ic501961d | Inorg. Chem. 2014, 53, 10731–10742

Table 5. Kinetics Parameters for the Phosphatase Activity of Complexes

complex	rate constant (s^{-1})	V_{max} (M s^{-1})	K_m (M)	R^a	k_{cat} (s^{-1})	catalytic efficiency E (M^{-1} s^{-1})
1	3.40×10^{-4}	6.38×10^{-8}	5.8×10^{-3}	0.9858	6.38×10^{-4}	0.11
3	1.32×10^{-3}	8.73×10^{-7}	2.8×10^{-3}	0.9904	8.73×10^{-3}	3.11
4	5.18×10^{-4}	5.62×10^{-7}	3.3×10^{-3}	0.9847	5.62×10^{-3}	1.7
5	3.50×10^{-4}	8.97×10^{-8}	3.7×10^{-3}	0.9893	8.97×10^{-4}	0.24

[a]Discrepancy value of the Lineweaver–Burk plot.

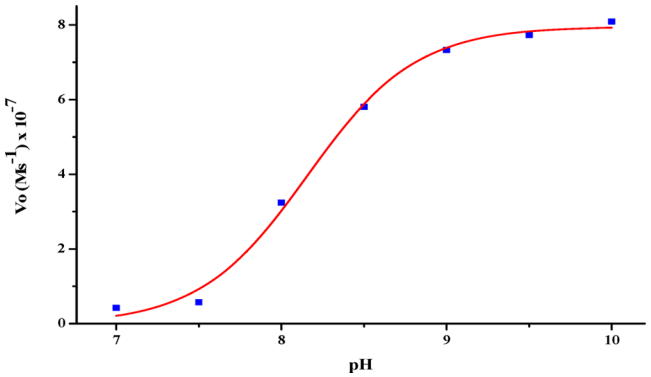

Figure 11. Dependence of the rate of HPNP transesterification on pH by complex $[Ni_2(L^2)(L^3)(CH_3CN)]$ (**3**). [complex] = 50 μM; [HPNP] = 5.0 mM in DMF–H_2O (30% v/v) at 25 °C.

undergoes nucleophilic attack by the metal-coordinated solvent generating a cyclic transition state. This transition state finally helps to cleave the P–O bond followed by the release of product in the form of *p*-nitrophenolate ion. Mikkola et al.[29] have reported different catalysis mechanisms for different model systems, depending upon both the catalyst and the substrate. The role of coordinated solvent such as water or alcohol in catalytic mechanism has been explored by many researchers.[30] Herein we report that a coordinated acetonitrile molecule in dinuclear complex **3** $[Ni_2(L^2)(L^3)(NCCH_3)]$ undergoes deprotonation of α-hydrogen to generate a reactive nucleophile. A similar nucleophilic behavior of metal-coordinated acetonitrile has also been observed by N. Kumagai et al.[31a] and Mayr et al.[31b] where the deprotonation of α-hydrogen of acetonitrile under basic conditions generates a nucleophile with a high catalytic efficiency. Consistently in complex **4**, deprotonation of coordinated water molecule generates hydroxide ion that acts as an active nucleophile. In the present complexes the nucleophilic attack of nickel-coordinated solvents to substrate results into the formation of cyclic phosphodiester product that further undergoes transesterifation to release *p*-nitrophenolate ion (Scheme 2). The formation of cyclic transition in the proposed mechanism was supported by NMR spectroscopy (Supporting Information, Figure S26). HPNP shows a signal at 5.17 ppm in ^{31}P NMR recorded in DMSO-d_6 (pH 8.5 in the presence of 0.1 M CHES buffer). The addition of 0.1 mM solution of complex **3** to a solution of substrate (2.5 mM) leads to the appearance of a new signal at 17.90 ppm corresponding to cyclic transition state.[21] Intensity of the substrate signal decreases gradually with progress of reaction and finally results in the disappearance of substrate signal at 5.17 ppm, on complete consumption of substrate.

To rationalize the observed relative performance of catalysts, various factors that affect the structure–activity relationship have been recognized, such as ligand–metal interaction, metal–metal distance, type of exogenous ligand, and coordination geometry around the metal ion.[32] Complexes **3** and **4** exhibited high phosphatase-like activity. A 3.9×10^5 and 2.5×10^5 times greater rate enhancement was observed for complex **3** and **4**, respectively, in comparison to uncatalyzed reaction ($k_{cat} = 2.26 \times 10^{-8}$ s^{-1}). In these dinuclear complexes coordinated acetonitrile and water molecule acts as nucleophile to catalyze the phosphate ester bond cleavage. A medium activity was observed in complex **5**, due to the coordinated DMF, which can be partially substituted by water molecule in aqueous condition. Complex **1** shows low phosphatase-like activity due to lack of appropriate coordinated solvent molecules. Moreover coordinated acetate groups inhibit the catalytic performance as at higher pH acetate ions are no longer coordinated to the complexes and are prone to be released during catalytic reaction. A similar observation has also been reported by Greatti et al.[33] To study the effect of acetate concentration on the catalytic activity, the rate of reaction was monitored as a function of acetate ion concentration for complex **1**. The results of catalytic activity were compared with and without acetate ion under similar experimental conditions. It was found that acetate ion significantly inhibits the catalytic activity, as evident from the plot of percentage inhibition (percentage inhibition = [(normal activity − inhibited activity)/(normal activity)] ×

Scheme 2

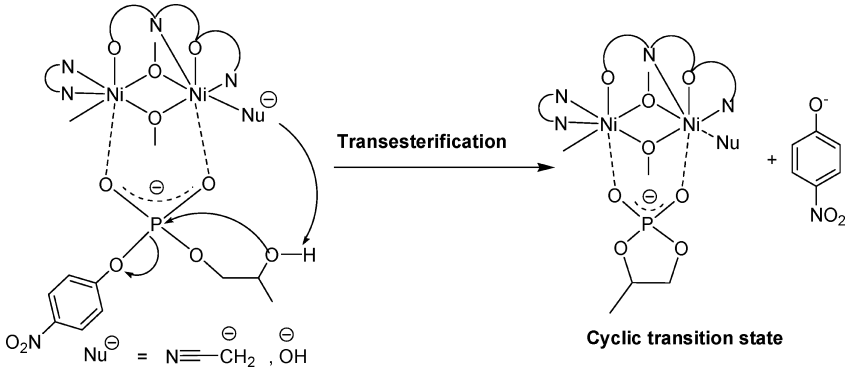

dx.doi.org/10.1021/ic501961d | Inorg. Chem. 2014, 53, 10731–10742

100) versus concentration of acetate ion (Supporting Information, Figure S27). The mononuclear Ni(II) complex **6** has very low activity due to lack of potential nucleophile and cooperative catalysis.[34] Mononuclear complexes are considered to be less relevant for mimicking the catalytic activity than their dinuclear analogues. In dinuclear complexes both the metal ions participate in the catalytic process; that is, one metal ion provides the nucleophile and the other cooperatively participates in substrate binding followed by cleavage. At the same time, metal−metal distance in the dinuclear complexes also exhibits a significant influence on the activity, owing to the fact that a distance of 2.9−3.2 Å is appropriate for the cooperative action.[34d,35] Consequently, it is worthwhile to compare the Ni(II)−Ni(II) distances in complexes **3** and **4** to explain their relative activity. In complex **3** the Ni(II)−Ni(II) distance is 3.18 Å in comparison to ∼5.72 Å expected for complex **4**, and as a result latter shows less catalytic activity due to lack of cooperative action. The negligible activity of complex **2** can be attributed to the rigid ligand−metal interaction with six bridging oxygen and nonavailability of vacant coordination site or labile group. This provides high rigidity and stability to the complex making the system less reactive with low catalytic activity.

SUMMARY

A series of tri-, di-, and mononuclear Ni(II) complexes were synthesized from tripodal and dipodal ligands with variable denticity. The reduction of denticity from tripodal to dipodal ligand favors the exogenous binding of solvent or/and anion to complete the coordination sites of Ni(II) center. The X-ray crystal structure analysis of complexes **2**, **3**, and **5** has reinforced this expectation. The physiochemical studies of complexes **1** and **4** have confirmed the presence of acetate and water in their coordination sphere. Complex **4** was crystallized in DMF, where DMF has displaced the coordinated water as a complex **5**. In addition a mononuclear complex **6** has also been synthesized and characterized to compare its activity with other tri- and dinuclear complexes. The structures of all the complexes have also been supported with electrochemical studies. The influence of ligand denticity and coordinating solvents/anions on the catalytic activities (DNA binding followed by phosphate ester cleavage) has been studied.

The DNA binding results show that all the complexes exhibit DNA binding ability through electrostatic interactions. The trinuclear complex **2** has highest value of binding constant due to its rigidity that favors the stronger interaction between complex and DNA, whereas complex **6** has lowest value of binding constant due to its mononuclear structure and nonrigid nature. In complex **4**, the deprotonation of two coordinated water molecules (OH^-) decreases the charge on central metal ion, and as a result a somewhat smaller value of DNA binding constant was observed. The dinuclear complexes **3** and **4** show high phosphatase-like activity due to coordinated solvent molecules that act as the nucleophile to catalyze the cleavage of phosphate ester bond. However, complex **3** shows higher activity than **4** due to smaller metal−metal distance that favors the cooperative action between two metal centers. Complex **1** shows low activity due to the presence of coordinated acetate group that inhibits the cleavage reaction. The mononuclear Ni(II) complex **6** has very low activity due to lack of appropriate nucleophile and cooperative catalysis. Complex **2** has negligible activity due to strong ligand−metal interaction and nonavailability of vacant coordination site or labile coordinating groups. Although binding is an important step in phosphate ester bond cleavage, the results showed that complex **2** has lowest cleavage activity in spite of strong binding. On the contrary, complexes **3** and **4** having coordinating solvents showed high catalytic activity. Thus, it can be inferred that binding is an essential but not the only condition for ester cleavage reactions; however, binding accompanied by appropriate metal−metal distance and nucleophilic attack of coordinated solvent, facilitate the phosphate ester bond cleavage in these complexes.

ASSOCIATED CONTENT

Supporting Information

X-ray crystallographic data in CIF format of complexes **2**, **3**, and **5**, ORTEP diagrams, kinetics plots, IR, ESI-MS, and NMR spectroscopic data is available. This material is available free of charge via the Internet at http://pubs.acs.org. Related crystallographic information can be obtained from the CCDC via www.ccdc.cam.ac.uk/data_request/cif (CCDC Nos. 1011103, 1018562, and 1011104 for **2**, **3**, and **5**, respectively).

AUTHOR INFORMATION

Corresponding Author

*E-mail: vimalb@iitrpr.ac.in. Phone: +91-1881242271.

Notes

The authors declare no competing financial interest.

ACKNOWLEDGMENTS

This work is supported by INSPIRE Faculty Research Grant No. IFA-11CH-09 from Department of Science and Technology (DST), Government of India. V.K.B. is also thankful to Indian Institute of Technology, Ropar (I.I.T. Ropar), for infrastructure and research facilities.

REFERENCES

(1) Fujita, E.; Brunschwig, B. S.; Ogata, T.; Yanagida, S. *Coord. Chem. Rev.* **1994**, *132*, 195.

(2) (a) De Clercq, B.; Verpoort, F. *Macromolecules* **2002**, *35*, 8943. (b) Nguyen, A. D.; Rail, M. D.; Shanmugam, M.; Fettinger, J. C.; Berben, L. A. *Inorg. Chem.* **2013**, *52*, 12847. (c) Midoes, A. C. D.; Aranha, P. E.; dos Sontos, M. P.; Tozzo, E.; Romera, S.; de A. Santos, R. H.; Dockal, E. R. *Polyhedron* **2008**, *27*, 59. (d) Opstal, T.; Verpoort, F. *Angew. Chem., Int. Ed.* **2003**, *42*, 2876. (e) Srinivasan, K.; Michaud, P.; Kochi, J. K. *J. Am. chem. Soc.* **1986**, *108*, 2309. (f) Dixit, P. S.; Srinivasan, K. *Inorg. Chem.* **1988**, *27*, 4507. (g) Rihter, B.; Srihari, S.; Hunter, S.; Masnovi, J. *J. Am. Chem. Soc.* **1993**, *115*, 3918.

(3) Molenveld, P.; Engbersen, J. F. J.; Reinhoudt, D. N. *Chem. Soc. Rev.* **2000**, *29*, 75.

(4) Strater, N.; Lipscomb, W. N.; Klablunde, T.; Krebs, B. *Angew. Chem., Int. Ed. Engl.* **1996**, *35*, 2024.

(5) (a) Dugas, H. *Bioorganic Chemistry;* Springer-Verlag: New York, 1988. (b) Vanhooke, J. L.; Benning, M. M.; Raushel, F. M.; Holden, H. M. *Biochemistry* **1996**, *35*, 6020.

(6) (a) Bazzicalupi, C.; Bencini, A.; Bianchi, A.; Fusi, V.; Giorgi, C.; Paoletti, P.; Valtancoli, B.; Zanchi, D. *Inorg. Chem.* **1997**, *36*, 2784. (b) Koike, T.; Inoue, M.; Kimura, E.; Shiro, M. *J. Am. Chem. Soc.* **1996**, *118*, 3091. (c) Yashiro, M.; Ishikubo, A.; Komiyama, M. *J. Chem. Soc., Chem. Commun.* **1997**, 83. (d) Chapman, W. H.; Breslow, R. *J. Am. Chem. Soc.* **1995**, *117*, 5462. (e) Yashiro, M.; Ishikubo, A.; Komiyama, M. *J. Chem. Soc., Chem. Commun.* **1995**, 1793. (f) Molenveld, P.; Kapsabelis, S.; Engbersen, J. F. J.; Reinhoudt, D. N. *J. Am. Chem. Soc.* **1997**, *119*, 2948. (g) Yamaguchi, K.; Akagi, F.; Fujinami, S.; Suzuki, M.; Shionoya, M.; Suzukia, S. *Chem. Commun.* **2001**, 375. (h) Mandal, S.; Balamurugan, V.; Lloret, F.; Mukherjee, R. *Inorg. Chem.* **2009**, *48*, 7544. (i) Diez-Castellnou, M.; Mancin, F.; Scrimin, P. *J. Am. Chem.*

Soc. **2014**, *136*, 1158. (j) Adhikary, J.; Chakraborty, P.; Das, S.; Chattopadhyay, T.; Bauza, A.; Chattopadhyay, S. K.; Ghosh, B.; Mautner, F. A.; Frontera, A.; Das, D. *Inorg. Chem.* **2013**, *52*, 13442.
(7) (a) Mukherjee, J.; Mukherjee, R. *Inorg. Chim. Acta* **2002**, *337*, 429. (b) Mancin, F.; Tecilla, P. *New J. Chem.* **2007**, *31*, 800. (c) Guha, A.; Chattopadhyay, T.; Paul, N. D.; Mukherjee, M.; Goswami, S.; Mondal, T. K.; Zangrando, E.; Das, D. *Inorg. Chem.* **2012**, *51*, 8750. (d) Anbu, S.; Kandawamy, M.; Varghese, B. *Dalton Trans.* **2010**, *39*, 3823.
(8) (a) Bhardwaj, V. K.; Aliaga-Alcalde, N.; Corbella, M.; Hundal, G. *Inorg. Chim. Acta* **2010**, *363*, 97. (b) Bhardwaj, V. K.; Hundal, M. S.; Corbella, M.; Gómez, V.; Hundal, G. *Polyhedron* **2012**, *38*, 224.
(9) Panja, A.; Matsuo, T.; Nagao, S.; Hirota, S. *Inorg. Chem.* **2011**, *50*, 11437.
(10) Mustapha, M.; Busche, C.; Reglinski, J.; Kennedy, A. R. *Polyhedron* **2011**, *30*, 1530.
(11) Mustapha, A.; Reglinski, J.; Kennedy, A. R.; Armstrong, D. R.; Sassmannshausen, J.; Murrie, M. *Inorg. Chem.* **2010**, *49*, 5350.
(12) Brown, D. M.; Usher, D. A. *J. Chem. Soc.* **1965**, 6558.
(13) Schilf, W.; Kamieński, B.; Kołodziej, B.; Grech, E. *J. Mol. Struct.* **2004**, *708*, 33.
(14) Cortés-Lozada, A.; Gómez, E.; Hernández, S. *Synth. React. Inorg., Met.-Org., Nano-Met. Chem.* **2012**, *42*, 1143.
(15) Altomare, A.; Burla, M. C.; Camalli, M.; Cascarano, G. L.; Giacovazzo, C.; Guagliardi, A.; Moliterni, A. G. G.; Polidori, G.; Spagna, R. *J. Appl. Crystallogr.* **1999**, *32*, 115.
(16) Sheldrick, G. M. *Acta Crystallogr., Sect. A* **2008**, *64*, 112.
(17) Farrugia, L. J. *J. Appl. Crystallogr.* **1999**, *32*, 837.
(18) Nardelli, M. *J. Appl. Crystallogr.* **1995**, *28*, 659.
(19) (a) Pennington, W. T. *J. Appl. Crystallogr.* **1999**, *32*, 1028. (b) Dolomanov, O. V.; Bourhis, L. J.; Gildea, R. J.; Howard, J. A. K.; Puschmann, H. *J. Appl. Crystallogr.* **2009**, *42*, 339.
(20) Reichmann, M. E.; Rice, S. A.; Thomas, C. A.; Doty, P. *J. Am. Chem. Soc.* **1954**, *76*, 3047.
(21) Selmeczi, K.; Michel, C.; Milet, A.; Gautier-Luneau, I.; Philouze, C.; Pierre, J.-L.; Schnieders, D.; Rompel, A.; Belle, C. *Chem.—Eur. J.* **2007**, *13*, 9093.
(22) (a) Nakamoto, K. *Infrared and Raman Spectra of Inorganic and Coordination Compounds,* 4th ed.; John Wiley & Sons: New York, 1986, 91. (b) Bellamy, L. J. *The Infra-Red Spectra of Complex Molecules;* John Wiley & Sons, Inc.: New York, 1966. (c) Deacon, G. B.; Philips, R. J. *Coord. Chem. Rev.* **1980**, *33*, 227.
(23) Lever, A.B.P. *Inorganic Electronic Spectroscopy;* Elsevier: Amsterdam, 1984.
(24) Anbu, S.; Kandaswamy, M.; Sudhakaran, P.; Murugan, V.; Varghese, B. *J. Inorg. Biochem.* **2009**, *103*, 401.
(25) Lutterman, D. A.; Chouai, A.; Liu, Y.; Sun, Y.; Stewart, C. D.; Dunbar, K. R.; Turro, C. *J. Am. Chem. Soc.* **2008**, *130*, 1163.
(26) Qian, W.; Gu, F.; Gao, L.; Feng, S.; Yan, D.; Liao, D.; Cheng, P. *Dalton Trans.* **2007**, 1060.
(27) Akine, S.; Taniguchi, T.; Nabeshima, T. *Inorg. Chem.* **2004**, *43*, 6142.
(28) Zhao, Y.; Zhu, J.; He, W.; Yang, Z.; Zhu, Y.; Li, Y.; Zhang, J.; Guo, Z. *Chem.—Eur. J.* **2006**, *12*, 6621.
(29) Korhonen, H.; Koivusalo, T.; Toivola, S.; Mikkola, S. *Org. Biomol. Chem.* **2013**, *11*, 8324.
(30) Daumann, L. J.; Dalle, K. E.; Schenk, G.; McGeary, R. P.; Bernhardt, P. V.; Ollis, D. L.; Gahan, L. R. *Dalton Trans.* **2012**, *41*, 1695. (b) Chen, J. W.; Wang, X. Y.; Zhu, Y. G.; Lin, J.; Yang, X. L.; Li, Y. Z.; Lu, Y.; Guo, Z. J. *Inorg. Chem.* **2005**, *44*, 3422. (c) Bazzicalupi, C.; Bencini, A.; Berni, E.; Bianchi, A.; Fedi, V.; Fusi, V.; Giorgi, C.; Paolettti, P.; Valtancoli, B. *Inorg. Chem.* **1999**, *38*, 4115.
(31) (a) Naoya Kumagai, N.; Matsunaga, S.; Shibasaki, M. *Tetrahedron* **2007**, *63*, 8598. (b) Minegishi, S.; Kobayashi, S.; Mayr, H. *J. Am. Chem. Soc.* **2004**, *126*, 5174.
(32) Koval, I. A.; Gamez, P.; Belle, C.; Selmeczi, K.; Reedijk, J. *Chem. Soc. Rev.* **2006**, *35*, 814.
(33) Greatti, A.; Scarpellini, M.; Peralta, R. A.; Casellato, A.; Bortoluzzi, A. J.; Xavier, F. R.; Jovito, R.; de Brito, M. A.; Szpoganicz, B.; Tomkowicz, Z.; Rams, M.; Haase, W.; Neves, A. *Inorg. Chem.* **2008**, *47*, 1107.
(34) (a) Koiket, T.; Kimura, E. *J. Am. Chem. Soc.* **1991**, *113*, 8935. (b) Subat, M.; Woinaroschy, K.; Gerstl, C.; Sarkar, B.; Kaim, W.; Konig, B. *Inorg. Chem.* **2008**, *47*, 4661. (c) Anbu, S.; Kamalraj, S.; Varghese, B.; Muthumary, J.; Kandaswamy, M. *Inorg. Chem.* **2012**, *51*, 5580. (d) Sanyal, R.; Guha, A.; Ghosh, T.; Mondal, T. K.; Zangrando, E.; Das, D. *Inorg. Chem.* **2014**, *53*, 85.
(35) Karlin, K. D.; Gultneh, Y.; Nicholson, T.; Zubieta, J. *Inorg. Chem.* **1985**, *24*, 3725.